Interfacial Dzyaloshinskii-Moriya interaction of antiferromagnetic materials

Md. Rakibul Karim Akanda,* In Jun Park, and Roger K. Lake†
Department of Electrical and Computer Engineering, University of California Riverside, California 92521, USA

(Received 19 June 2020; revised 20 October 2020; accepted 24 November 2020; published 15 December 2020)

The interface between a ferromagnet (FM) or antiferromagnet (AFM) and a heavy metal (HM) results in an antisymmetric exchange interaction known as the interfacial Dzyaloshinskii-Moriya interaction (iDMI) which favors noncollinear spin configurations. The iDMI is responsible for stabilizing noncollinear spin textures such as skyrmions in materials with bulk inversion symmetry. Interfacial DMI values have been previously determined theoretically and experimentally for FM/HM interfaces, and, in this work, they are calculated for the metallic AFM MnPt and the insulating AFM NiO. The heavy metals considered are W, Re, and Au. Values for the iDMI, exchange, and anisotropy constants are determined for different AFM and HM thicknesses. The iDMI values of the MnPt heterolayers are comparable to those of the common FM materials, and those of NiO are lower. In few-layer films of (001) MnPt, the high spin orbit coupling of the Pt layers can give rise to a small DMI in the absence of a HM layer.

DOI: 10.1103/PhysRevB.102.224414

I. INTRODUCTION

Antiferromagnetic (AFM) materials are of current interest due to their insensitivity to external magnetic fields, absence of demagnetizing fields, scalability to small dimensions, widespread availability in nature with high Néel temperatures, and operation in the THz frequency range [1–8]. Antiferromagnetic materials exhibit various interesting phenomena such as a large anomalous Hall effect, spin Seebeck effect, spin Hall magnetoresistance, and spin galvanic effects [9–21]. They offer various promising spintronic applications exploiting skyrmions or domain walls which can be used as nonvolatile memory and racetrack memory [22–29].

Noncollinear spin configurations such as skyrmions and chiral helices are found in noncentrosymmetric materials with broken inversion symmetry [30–32]. Since noncentrosymmetric magnetic materials are not common in nature, heterolayers consisting of a heavy metal (HM), which offers high spin orbit coupling (SOC), and a magnetic material can be created that breaks inversion symmetry at the interface. At an HM/FM or HM/AFM interface, the interfacial Dzyaloshinskii-Moriya interaction (iDMI), which is an antisymmetric exchange interaction, can stabilize Néel type domain walls and skyrmions [33–43]. The interfacial DMI of FM materials is generally measured using Brillouin light scattering (BLS) [44–50]. Experimentally AFM spin textures are measured using spin polarized scanning tunneling microscopy (STM), and the bulk DMI in noncentrosymmetric materials is measured using inelastic neutron scattering [51,52].

There have been prior theoretical and experimental studies of iDMI in engineered or synthetic antiferromagnetic systems [53–56]. In Refs. [55,56], spin-polarized scanning tunneling microscopy was used to study heterostructures of monolayer Mn on W(110) and Re(0001), and the iDMI was calculated using density functional theory (DFT). The same theoretical approach was used to study the iDMI of Fe/Ir bilayers on Rh(001) [53]. In Ref. [54], the two-dimensional AFM-Rashba model was introduced to calculate the iDMI in 2D Rashba AFMs.

This paper describes the results of *ab initio* calculations of the iDMI for three different material combinations of HMs and AFMs. Since the iDMI helps to stabilize Néel type skyrmions in which spins rotate from out-of-plane to in-plane, the AFM materials MnPt and NiO are chosen with Néel vectors oriented out-of-plane [57–61]. Also, both MnPt and NiO have high Néel temperatures (975 K and 530 K, respectively) [62–64], which are required for on-chip applications. MnPt has a stripe-type AFM spin texture, and NiO has a G-type AFM spin texture. Creating heterolayers for density functional theory (DFT) calculations requires lattice matching to create a periodic structure. This generally requires choosing materials with lattice constants that are relatively close to minimize strain. For this reason, the two HMs paired with MnPt are tungsten (W) and rhenium (Re), and the HM paired with NiO is gold (Au). MnPt-W has a lattice mismatch of 1.49%, MnPt-Re has a mismatch of 1.25%, and NiO-Au has a mismatch of 0.7%. The effects of thickness variation of the AFM layer and the heavy metal layer on the iDMI are discussed. The magnetic moments, magnetizations, exchange constants, and magnetic anisotropy constants are also calculated as functions of layer thicknesses. These values provide required input parameters for micromagnetic modeling of AFM spin textures.

II. METHOD

The interfacial DMI is evaluated using first principles calculations based on the Vienna *ab initio* simulation package

*makan001@ucr.edu
†Corresponding author: rlake@ece.ucr.edu

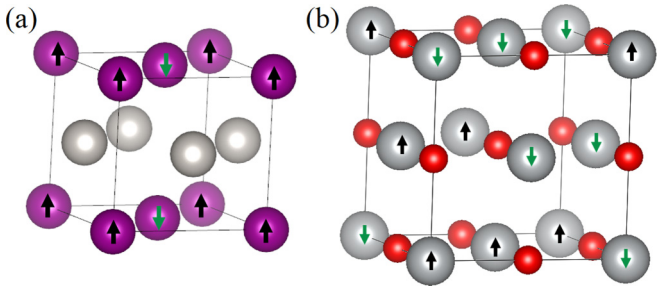

FIG. 1. (a) Unit cell of MnPt having stripe-type AFM spin configurations. (b) Unit cell of NiO having G-type AFM spin configurations. Spin directions are shown in 3*d* orbital magnetic materials (Mn or Ni) and atoms without spin are Pt (gray) and oxygen (red).

(VASP) [65]. The electron-core interactions are described by the projected augmented wave (PAW) potentials [66], and the exchange correlation energy is included with the generalized gradient approximation (GGA) parameterized by Perdew-Burke-Ernzerhof (PBE) [67]. The cutoff energy for the plane wave basis is 550 eV in all calculations. The Monkhorst-Pack scheme is used with Γ-centered $10\times10\times1$ *k*-point grids to make sure the total energy is converged within 10^{-5} eV per unit cell.

For calculations of the iDMI, the unit cells in Fig. 1 are repeated as shown in Fig. 2, so that spin orientations can be rotated in clockwise (CW) and counterclockwise (CCW) directions [68–70]. MnPt and W (or Re) unit cells are repeated four times to make a supercell ($4\times1\times1$) in which spins of the Mn atoms are rotated one period over the length of the supercell as shown in Fig. 3(a). A vacuum layer of 15 Å is added along the out-of-plane direction. NiO and Au unit cells are repeated to make a supercell ($2\times2\times1$) in which the spins of the Ni atoms are rotated once over the length of the supercell as shown in Fig. 3(b).

Calculations are performed in three steps to find the interfacial Dzyaloshinskii-Moriya interaction [68–70]. The supercell structure is relaxed until the forces are smaller than 0.01 eV/Å to determine the most stable interfacial geometries. Table I shows the relaxed interlayer distances between the interfacial atoms of the magnetic layer and the heavy metal layer. Next, the Kohn-Sham equations are solved without spin orbit coupling (SOC) to determine the charge distribution of the system's ground state. Finally, spin orbit coupling (SOC) is included and the total energy of the system is determined for the CW and CCW spin spirals having 90 degree rotation. The total DMI strength, D_{tot}, is found from the energy difference between the CW and CCW spin configurations [68].

The iDMI is calculated using the approach of Yang *et al.* [68] generalized for an AFM system. The energy due to the Dzyaloshinskii-Moriya interaction can be written as

$$E_{\text{DMI}} = \sum_{\langle i,j\rangle} \mathbf{d}_{ij} \cdot [\mathbf{S}_i \times \mathbf{S}_j], \tag{1}$$

where $\mathbf{d}_{ij}$ is the DMI vector and $\mathbf{S}_i$ is the unit vector of a magnetic moment. $\mathbf{d}_{ij}$ is found from $d(\hat{\mathbf{z}}\times\hat{\mathbf{u}}_{ij})$, where $\hat{\mathbf{u}}_{ij}$ is the unit vector between sites i and j, and $\hat{\mathbf{z}}$ is the direction normal to the film which is oriented from the heavy metal to the magnetic film [68].

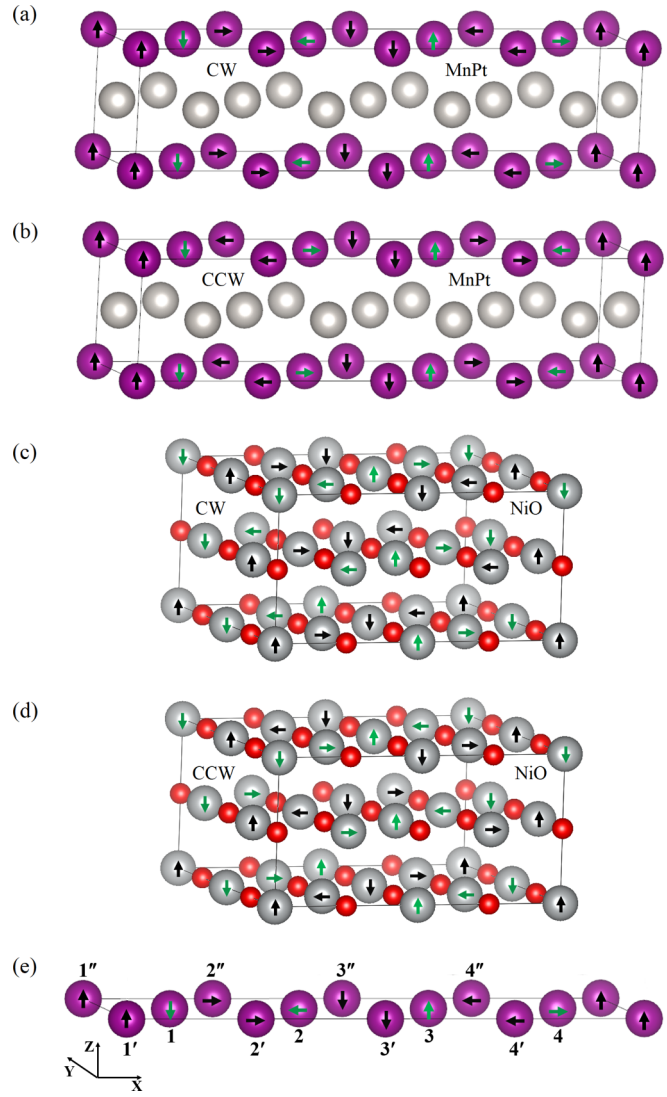

FIG. 2. Spiral spin configurations used in the DMI calculations for (a), (b), (e) MnPt and (c), (d) NiO. A $4\times1\times1$ unit cell supercell of MnPt is constructed with a spin spiral in the (a) clockwise and (b) counterclockwise directions. A $2\times2\times1$ unit cell supercell of NiO is constructed with a spin spiral in the (c) clockwise and (d) counterclockwise directions. (e) Clockwise rotated spin configuration in one layer of MnPt with labels used in Eq. (2).

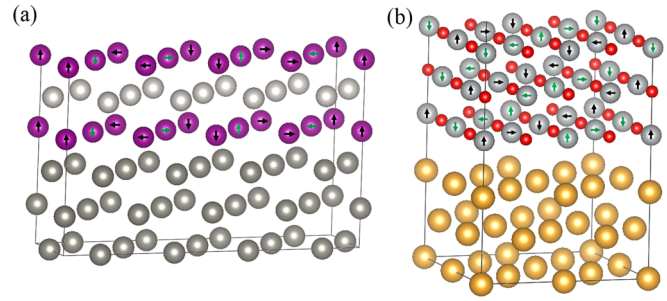

FIG. 3. (a) MnPt on top of W. Mn atoms are purple. (b) NiO on top of Au. Oxygen atoms are red.

TABLE I. Interlayer distances in the system of three layers of MnPt on top of three layers of W or Re and in the system of three layers of NiO on top of three layers of Au.

Interlayer	Distance (Å)
Mn-Pt	1.85
Mn-Re	1.84
Mn-W	1.81
Ni-Ni	2.09
Ni-Au	2.59

To numerically determine the value of d, AFM Nèel-vector spirals are created in a supercell. Figure 2(e) illustrates such a spiral along the x direction. The spins that form the antialigned spin pairs of the AFM primitive cells are numbered 1,1′, 2,2′, 3,3′, and 4,4′. Each pair is successively rotated 90° with respect to the pair on the left. The local magnetization of each primitive cell remains zero. Writing out the sum in Eq. (1) over the four nearest neighbors of atom 2, the energy of atom 2 is

$$E_2 = \tfrac{1}{2}[\mathbf{d}_{22'}\cdot(\mathbf{S}_2\times\mathbf{S}_{2'}) + \mathbf{d}_{22''}\cdot(\mathbf{S}_2\times\mathbf{S}_{2''}) + \mathbf{d}_{23'}\cdot(\mathbf{S}_2\times\mathbf{S}_{3'}) + \mathbf{d}_{23''}\cdot(\mathbf{S}_2\times\mathbf{S}_{3''})] + E_{\text{other}}, \quad (2)$$

where E_{other} is the spin independent, anisotropy, and symmetric exchange energy contributions. The first two terms, 2,2′ and 2,2″, on the right side of Eq. (2) are zero due to parallel or antiparallel magnetic moments in the cross products. The 2,2′ term is an intra primitive cell term, and atom 2″ is equivalent to atom 2′ but in the next primitive cell in the y direction. The nonzero terms come from the two nearest neighbor pairs 2,3′ and 2,3″ resulting in

$$E_2 = \frac{1}{2}\left[\frac{1}{\sqrt{2}}D_{\text{tot}} + \frac{1}{\sqrt{2}}D_{\text{tot}}\right] + E_{\text{other}}, \quad (3)$$

where the factors of $\frac{1}{\sqrt{2}}$ are due to the 45° angle between $\mathbf{d}_{23'}$ and $\mathbf{S}_2\times\mathbf{S}_{3'}$. D_{tot} is the total DMI strength which is considered as the DMI strength concentrated in a single atomic layer [68]. The energies of atom 2 resulting from CW and CCW spirals are

$$E_{2,\text{CW}} = \frac{1}{\sqrt{2}}D_{\text{tot}} + E_{\text{other}} \quad (4)$$

$$E_{2,\text{CCW}} = -\frac{1}{\sqrt{2}}D_{\text{tot}} + E_{\text{other}}. \quad (5)$$

A single Mn layer of a supercell that contains eight magnetic atoms is shown in Fig. 2(e). Note that the last line of atoms along the x and y directions are repeated and belong to the next supercell, and are therefore not counted. For the Mn layer of Fig. 2(e),

$$\Delta E_{\text{DMI}} = (E_{\text{CW}} - E_{\text{CCW}}) = 8\sqrt{2}D_{\text{tot}}, \quad (6)$$

so that D_{tot} is

$$D_{\text{tot}} = (E_{\text{CW}} - E_{\text{CCW}})/m, \quad (7)$$

where $m = 8\sqrt{2}$ for both MnPt and NiO. From D_{tot}, we determine the micromagnetic DMI, D_μ, which is the parameter used in micromagnetic simulations. Considering four nearest neighbors, D_μ is found from [68]

$$D_\mu = \frac{4D_{\text{tot}}}{N_L a^2}, \quad (8)$$

where a is the lattice constant, and N_L is the number of magnetic layers.

This approach for determining iDMI values has been used in several different studies and applied to different heterostructure systems [68–70]. The approach assumes that the iDMI can be described in a nearest neighbor approximation. It results in a minimal length periodic spin spiral and minimal size supercell as shown in Fig. 2. There are other approaches. Longer spin spirals with smaller angles can be used, however the supercells quickly become extremely large. For example, with 30° between nearest neighbor spins, a three layer MnPt/three layer HM structure results in a supercell containing 216 atoms. Furthermore, in this approach, several different spin spirals with different nearest neighbor angles must be simulated and the resulting energies fitted to a parabolic curve to extract the iDMI [53,55,56,71,72]. Beyond the above two methods of creating spin spirals in supercells, there are several other approaches such as (i) the Korringa-Kohn-Rostoker (KKR) Green function method [73], (ii) the coned full potential linearized augmented plane wave generalized Bloch theorem (FLAPW-gBT) method [74,75], (iii) the flat FLAPW-gBT method [74,75], and (iv) the coned supercell spin spiral method [76]. Variations of the DMI values calculated from the different methods have been studied [76]. Compared to the approach used in this work, the KKR method varied by 6.7%, the coned FLAPW-gBT method varied by 23%, the flat FLAPW-gBT method varied by 21%, and the coned supercell method varied by 6.8% for monolayer Co on Pt [76]. Several papers containing both experimental and theoretical results showed that the method used in this paper provides DMI values which are comparable to experimental results for different systems [70,77].

The magnetic moment and magnetization are calculated from the collinear AFM spin configurations of the three different combinations of materials where the magnetization is the magnetic moment per unit volume. The magnetic anisotropy energy is calculated from the energy difference between the in plane and out of plane spin configurations of MnPt [77].

The exchange energy (J) is calculated from the total energy difference between collinear antiferromagnetic (E_{AFM}) and ferromagnetic (E_{FM}) configurations [76,78–80]. With four nearest neighbors, the nearest-neighbor exchange energy is found from VASP [79,80],

$$J = \frac{E_{\text{AFM}} - E_{\text{FM}}}{8}. \quad (9)$$

The micromagnetic exchange stiffness (A) is related to J by [76,78]

$$A = \frac{1}{2V_\Omega}\sum_j J_{0j}(R_{0j})^2, \quad (10)$$

where V_Ω is the volume of the primitive AFM unit cell, $R_{0j} = \frac{a}{\sqrt{2}}$ is the distance between nearest-neighbor magnetic atoms, and a is the lattice constant of the primitive AFM unit cell. For

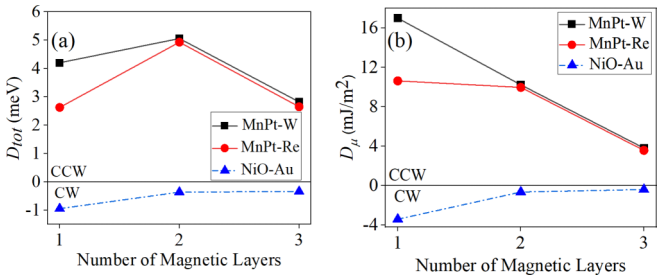

FIG. 4. (a) D_{tot} and (b) D_μ of MnPt-W, MnPt-Re, and NiO-Au as a function of the thickness of the AFM. The thickness of the HM is fixed at three layers. Positive DMI indicates that the CCW spin spiral is the lower energy state.

four nearest neighbors, the micromagnetic parameter is [76]

$$A = \frac{a^2 J}{N_L V_\Omega}. \tag{11}$$

III. RESULTS

Calculated values of D_{tot} and D_μ for MnPt-Re, MnPt-W, and NiO-Au as a function of AFM layer number are shown in Fig. 4. The structures consist of the AFM layers on top of three layers of HM. The trends and quantitative values are similar to those in HM/FM interfaces [81]. For a monolayer of MnPt, the strength of the iDMI, in terms of D_{tot}, is larger with W than with Re, and this is consistent with the fact that the SOC of W is larger than that of Re. Both MnPt-W and MnPt-Re show larger iDMI compared to that of NiO-Au, and this is consistent with the fact that the magnetic moment of Mn is larger than that of Ni. The trend that higher magnetic moments provide larger interfacial DMI following Hund's rule [81] is also observed in HM/FM interfaces.

The magnitude of the volume averaged interfacial DMI (D_μ), shown in Fig. 4(b), decreases with increasing thickness of the AFM material, and it will eventually approach zero for thick magnetic material [68,82]. However, this does not necessarily hold true for the first two to three layers in terms of the total DMI strength D_{tot}, as shown in Fig. 4(a). In MnPt, each layer of magnetic atoms (Mn) is sandwiched between layers of HM atoms (Pt). Thus, D_{tot} depends not only on the spin orbit coupling (SOC) arising from the interfacial heavy metal W (or Re), but also on the SOC from the inner heavy metal Pt, and the resulting total DMI strength initially varies nonmonotonically with layer number as shown in Fig. 4(a). In contrast, NiO contains no HM atoms, and the magnitude of D_{tot} decreases monotonically with thickness.

The iDMI values of antiferromagnetic materials are comparable to those of ferromagnetic materials. The iDMI of monolayer MnPt on W or Re is comparable to that of monolayer Fe sandwiched between Pd and Ir, which is well known for hosting nm scale skyrmions [83–85], and also to monolayer Co on Pt [84]. Three layers of MnPt on W has $D_\mu = 3.8$ mJ/m^2, which is comparable to that of three layers of Co on Pt [68,69]. Three layers of Ni on graphene has $D_\mu \approx 0.5$ mJ/m^2 [70], and three layers of AFM NiO on Au has an $D_\mu = 0.4$ mJ/m^2.

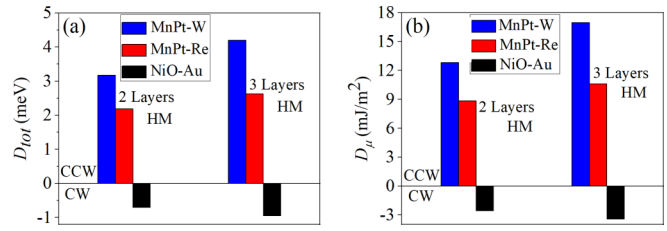

FIG. 5. iDMI of monolayer AFM for two different HM thicknesses: (a) D_{tot} with one magnetic layer and (b) D_μ.

A thicker heavy metal layer increases the iDMI, since increasing the thickness of the heavy metal layer initially increases the proximity SOC in the AFM. The increase in the iDMI with thickness of the HM layer is shown in Fig. 5. Since the HM provides proximity SOC, increasing the HM thickness from one layer to several layers increases the iDMI before it saturates after three or four layers [86].

Since the magnitude of the iDMI depends on the local magnetic moments, comparisons of the magnetic moments and saturation magnetizations of MnPt and NiO with three layers of heavy metal are shown in Fig. 6 as a function of the AFM thickness. The highest magnetic moment is shown. NiO has smaller magnetic moments than MnPt, which contributes to its lower iDMI compared to MnPt-W and MnPt-Re. Overall, the values are smaller than those of the bulk. The magnetic moments increase with increasing thicknesses of the AFM thin films, and they approach the bulk values of MnPt and NiO [87–89].

There are two reasons for smaller magnetic moments: (i) reduced thickness of the magnetic materials [90,91] and (ii) orbital hybridization at the AFM-HM interface [81]. The hybridization of the 3*d* orbitals of the AFM with the 5*d* orbitals of the HM reduces the magnetic moments of the AFM [92,93], and it gives rise to nonzero magnetic moments in the HM layer. In FM/HM systems, a higher proximity induced magnetic moment in the heavy metal reduces the iDMI [68], and this is consistent with what we observe with the AFM/HM

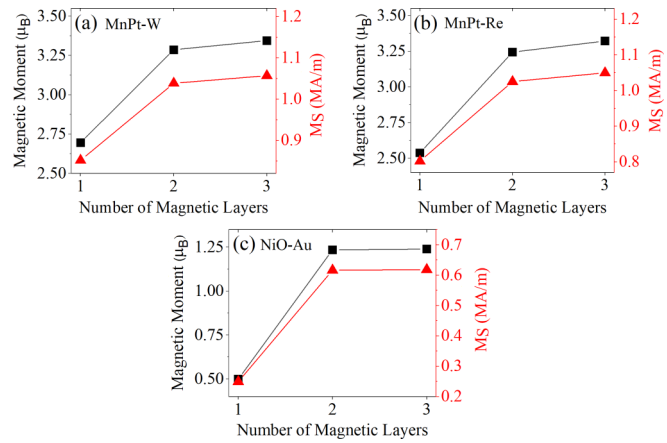

FIG. 6. Magnetic moments and saturation magnetization of (a) MnPt-W, (b) MnPt-Re, and (c) NiO-Au as a function of the thickness of the AFM. The thickness of the HM is fixed at three layers.

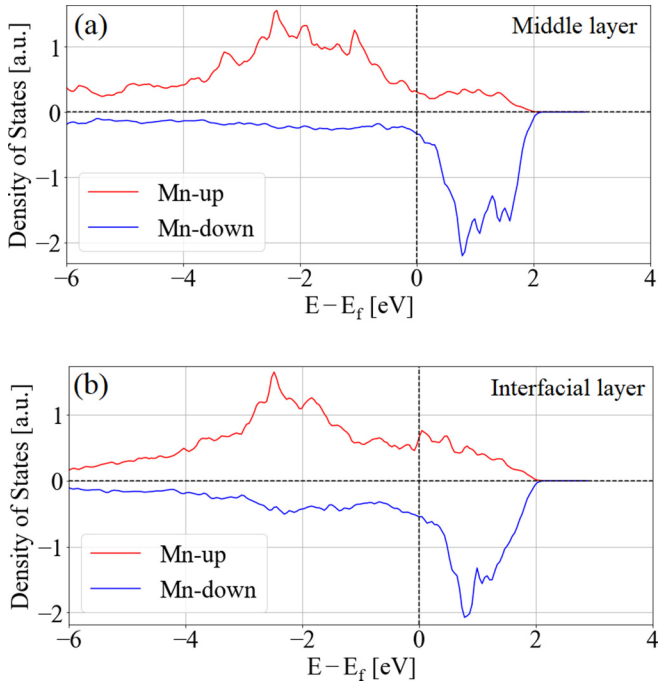

FIG. 7. Local density of states of Mn atom in three layers of MnPt on top of three layers of Re: (a) middle Mn atom which is far from Re, (b) bottom Mn atom which is close to Re and is affected by proximity induced magnetic moment.

system. One layer of MnPt on three layers of Re induces a proximity magnetic moment of 0.211 μ_B on the first layer of Re atoms, and one layer of MnPt on three layers of W induces a proximity magnetic moment of 0.206 μ_B on the first layer of W atoms. The enhanced magnetic moment in the HM is accompanied by a reduced magnetic moment in the interfacial magnetic atoms. For a system with three layers of MnPt on top of three layers of Re, the magnetic moment of a Mn atom at the HM interface is 2.18 μ_B, and the magnetic moment of a Mn atom in the middle layer is 3.13 μ_B. This effect is apparent in the spin-resolved local density of states (LDOS) of the Mn atoms. Figure 7 shows the spin-resolved LDOS of Mn atoms in the (a) middle layer and (b) interfacial layer from the heterostructure of three layers of MnPt on three layers of heavy metal (Re). The upper (red) and lower (blue) curves show the spin-up $D_\uparrow$ and spin-down $D_\downarrow$ LDOS, respectively. The magnetic moment is proportional to the integration of $D_\uparrow - D_\downarrow$ over the occupied energies $E \leqslant E_F$. The LDOS of the minority down spin is larger in the interfacial layer than in the middle layer, with the result that the Mn atoms at the interface are less polarized.

MnPt consists of alternating layers of magnetic Mn atoms and heavy metal Pt atoms with high SOC. A finite (001) slab of MnPt, consisting of an integer number of unit cells, breaks inversion symmetry since one face is a Mn layer and the opposing face is a Pt layer. The combination of high SOC and broken inversion symmetry gives rise to a small amount of DMI even without a proximity HM layer. For a three layer slab of MnPt with the Mn layer on the bottom and the Pt layer on the top, $D_{\text{tot}} = -1.02$ meV/$3d$ atom, and $D_\mu = -1.37$ mJ/m^2. In contrast, NiO does not contain any heavy metal

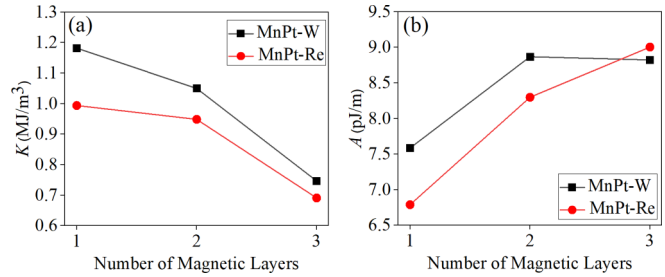

FIG. 8. (a) Magnetic anisotropy constant of MnPt with three layers of heavy metals. (b) Exchange stiffness of MnPt with three layers of heavy metals.

atoms, three layers remain geometrically inversion symmetric, and it exhibits zero DMI in the absence of an adjacent heavy metal layer.

Calculated values for the magnetocrystalline anisotropy constants and exchange stiffnesses are shown in Fig. 8 for different numbers of magnetic layers. The magnetic anisotropy constant decreases with thickness, and the exchange stiffness slightly increases with the number of layers, which is consistent with a previous study [77].

IV. CONCLUSIONS

The interfacial Dzyaloshinskii-Moriya interaction of MnPt/W, MnPt/Re, and NiO/Au are calculated for different thicknesses of both the AFM and the HM. Values of iDMI, magnetic moments, exchange and magnetic anisotropy constants required for the micromagnetic simulations are determined. The values of the iDMI of the MnPt/HM heterolayers are comparable to those of the common ferromagnetic materials such as Fe, Co, or CoFeB. The iDMI of the NiO/Au system is approximately a factor of 7 lower. In general, iDMI is maximized by choosing AFM materials with larger magnetic moments, heavy metals with high spin orbit coupling, thinner AFM layers from 1–3 monolayers, and HM thicknesses of at least three to four layers. Few layer (001) MnPt which contains both HM atoms and magnetic atoms exhibits an intrinsic DMI, albeit smaller than the iDMI induced by a proximity HM layer. These results and the quantitative values provided will help guide experimental realization and provide needed parameters for micromagnetic simulations of AFM materials with domain walls and skyrmions supported by iDMI.

ACKNOWLEDGMENTS

This work was supported as part of Spins and Heat in Nanoscale Electronic Systems (SHINES) an Energy Frontier Research Center funded by the US Department of Energy, Office of Science, Basic Energy Sciences under Award No. DE-SC0012670. This work used the Extreme Science and Engineering Discovery Environment (XSEDE) [94], which is supported by National Science Foundation Grant No. ACI-1548562 and allocation ID TG-DMR130081.

[1] V. Baltz, A. Manchon, M. Tsoi, T. Moriyama, T. Ono, and Y. Tserkovnyak, Rev. Mod. Phys. **90**, 015005 (2018).

[2] I. Žutić, J. Fabian, and S. D. Sarma, Rev. Mod. Phys. **76**, 323 (2004).

[3] D. D. Russell, A. J. Neer, B. C. Melot, and S. Derakhshan, Inorg. Chem. **55**, 2240 (2016).

[4] B. C. Melot, B. Paden, R. Seshadri, E. Suard, G. Nénert, A. Dixit, and G. Lawes, Phys. Rev. B **82**, 014411 (2010).

[5] A. J. Neer, J. A. Milam-Guerrero, J. E. So, B. C. Melot, K. A. Ross, Z. Hulvey, C. M. Brown, A. A. Sokol, and D. O. Scanlon, Phys. Rev. B **95**, 144419 (2017).

[6] Y. Hou and R. Wu, Nano Lett. **19**, 2472 (2019).

[7] O. Gomonay, T. Jungwirth, and J. Sinova, Physica Status Solidi (RRL) **11**, 1700022 (2017).

[8] S. A. Siddiqui, J. Sklenar, K. Kang, M. J. Gilbert, A. Schleife, N. Mason, and A. Hoffmann, J. Appl. Phys. **128**, 040904 (2020).

[9] S. Nakatsuji, N. Kiyohara, and T. Higo, Nature (London) **527**, 212 (2015).

[10] N. Kiyohara, T. Tomita, and S. Nakatsuji, Phys. Rev. Applied **5**, 064009 (2016).

[11] C. Sürgers, T. Wolf, P. Adelmann, W. Kittler, G. Fischer, and H. V. Löhneysen, Sci. Rep. **7**, 42982 (2017).

[12] S. M. Wu, W. Zhang, A. Kc, P. Borisov, J. E. Pearson, J. S. Jiang, D. Lederman, A. Hoffmann, and A. Bhattacharya, Phys. Rev. Lett. **116**, 097204 (2016).

[13] S. Seki, T. Ideue, M. Kubota, Y. Kozuka, R. Takagi, M. Nakamura, Y. Kaneko, M. Kawasaki, and Y. Tokura, Phys. Rev. Lett. **115**, 266601 (2015).

[14] J. B. S. Mendes, R. O. Cunha, Santos O. Alves, P. R. T. Ribeiro, F. L. A. Machado, Rodriguez L. R. Suárez, A. Azevedo, and S. M. Rezende, Phys. Rev. B **89**, 140406(R) (2014).

[15] S. M. Rezende, R. L. Rodríguezsuárez, and A. Azevedo, Phys. Rev. B **93**, 014425 (2016).

[16] A. Prakash, J. Brangham, F. Yang, and J. P. Heremans, Phys. Rev. B **94**, 014427 (2016).

[17] X. Zhou, L. Ma, Z. Shi, W. J. Fan, J. G. Zheng, R. F. L. Evans, and S. M. Zhou, Phys. Rev. B **92**, 060402(R) (2015).

[18] J. H. Han, C. Song, F. Li, Y. Y. Wang, G. Y. Wang, Q. H. Yang, and F. Pan, Phys. Rev. B **90**, 144431 (2014).

[19] W. Lin and C. L. Chien, Phys. Rev. Lett. **118**, 067202 (2017).

[20] J. Sinova, S. O. Valenzuela, J. Wunderlich, C. H. Back, and T. Jungwirth, Rev. Mod. Phys. **87**, 1213 (2015).

[21] H. Chen, Q. Niu, and A. H. MacDonald, Phys. Rev. Lett. **112**, 017205 (2014).

[22] J. Barker and O. A. Tretiakov, Phys. Rev. Lett. **116**, 147203 (2016).

[23] I. Raičević, D. Popović, C. Panagopoulos, L. Benfatto, M. B. Silva Neto, E. S. Choi, and T. Sasagawa, Phys. Rev. Lett. **106**, 227206 (2011).

[24] P. M. Buhl, F. Freimuth, S. Blügel, and Y. Mokrousov, Phys. Status Solidi **11**, 1700007 (2017).

[25] B. Göbel, A. Mook, J. Henk, and I. Mertig, Phys. Rev. B **96**, 060406(R) (2017).

[26] A. Salimath, F. Zhuo, R. Tomasello, G. Finocchio, and A. Manchon, Phys. Rev. B **101**, 024429 (2020).

[27] C. Chappert, A. Fert, and F. N. V. Dau, Nat. Mater. **6**, 813 (2007).

[28] C. Marrows, Science **351**, 558 (2016).

[29] S. S. P. Parkin, M. Hayashi, and L. Thomas, Science **320**, 190 (2008).

[30] S. Heinze, K. von Bergmann, M. Menzel, J. Brede, A. Kubetzka, R. Wiesendanger, G. Bihlmayer, and S. Blugel, Nat. Phys. **7**, 713 (2011).

[31] H. Du, D. Liang, C. Jin, L. Kong, M. J. Stolt, W. Ning, J. Yang, Y. Xing, J. Wang, R. Che, J. Zang, S. Jin, Y. Zhang, and M. Tian, Nat. Commun. **6**, 7637 (2015).

[32] N. Nagaosa and Y. Tokura, Nat. Nanotechnol. **8**, 899 (2013).

[33] A. Fert, V. Cros, and J. Sampaio, Nat. Nanotechnol. **8**, 152 (2013).

[34] O. Boulle, J. Vogel, H. Yang, S. Pizzini, D. de Souza Chaves, A. Locatelli, T. O. Menteş, A. Sala, L. D. B. Prejbeanu, O. Klein, M. Belmeguenai, Y. Roussigné, A. Stashkevich, S. M. Chérif, L. Aballe, M. Foerster, M. Chshiev, S. Auffret, I. M. Miron, and G. Gaudin, Nat. Nanotechnol. **11**, 449 (2016).

[35] S. Woo, K. Litzius, B. Krüger, M. Y. Im, L. Caretta, K. Richter, M. Mann, A. Krone, R. M. Reeve, M. Weigand, P. Agrawal, I. Lemesh, M. A. Mawass, P. Fischer, M. Kläui, and G. S. D. Beach, Nat. Mater. **15**, 501 (2016).

[36] W. Legrand, D. Maccariello, N. Reyren, K. Garcia, C. Moutafis, C. M. Luchaire, S. Collin, K. Bouzehouane, V. Cros, and A. Fert, Nano Lett. **17**, 2703 (2017).

[37] W. Legrand, D. Maccariello, F. Ajejas, S. Collin, A. Vecchiola, K. Bouzehouane, N. Reyren, V. Cros, and A. Fert, Nat. Mater. **19**, 34 (2020).

[38] X. Zhang, Y. Zhou, and M. Ezawa, Sci. Rep. **6**, 24795 (2016).

[39] C. B. Muratov, V. V. Slastikov, A. G. Kolesnikov, and O. A. Tretiakov, Phys. Rev. B **96**, 134417 (2017).

[40] V. V. Slastikov, C. B. Muratov, J. M. Robbins, and O. A. Tretiakov, Phys. Rev. B **99**, 100403(R) (2019).

[41] Y. Zhu, J. Fan, and R. Wu, J. Magn. Magn. Mater. **507**, 166805 (2020).

[42] W. Yu, J. Lan, R. Wu, and J. Xiao, Phys. Rev. B **94**, 140410(R) (2016).

[43] B. Zimmermann, W. Legrand, D. Maccariello, N. Reyren, V. Cros, S. Blügel, and A. Fert, Appl. Phys. Lett. **113**, 232403 (2018).

[44] L. Udvardi and L. Szunyogh, Phys. Rev. Lett. **102**, 207204 (2009).

[45] A. T. Costa, R. B. Muniz, S. Lounis, A. B. Klautau, and D. L. Mills, Phys. Rev. B **82**, 014428 (2010).

[46] J. H. Moon, S. M. Seo, K. J. Lee, K. W. Kim, J. Ryu, H. W. Lee, R. D. McMichael, and M. D. Stiles, Phys. Rev. B **88**, 184404 (2013).

[47] A. F. Volkov, F. S. Bergeret, and K. B. Efetov, Phys. Rev. B **99**, 144506 (2019).

[48] K. Di, V. L. Zhang, H. S. Lim, S. C. Ng, M. H. Kuok, J. Yu, J. Yoon, X. Qiu, and H. Yang, Phys. Rev. Lett. **114**, 047201 (2015).

[49] X. Ma, G. Yu, X. Li, T. Wang, D. Wu, K. S. Olsson, Z. Chu, K. An, J. Q. Xiao, K. L. Wang, and X. Li, Phys. Rev. B **94**, 180408(R) (2016).

[50] X. Ma, G. Yu, S. A. Razavi, S. S. Sasaki, X. Li, K. Hao, S. H. Tolbert, K. L. Wang, and X. Li, Phys. Rev. Lett. **119**, 027202 (2017).

[51] O. Gomonay, V. Baltz, A. Brataas, and Y. Tserkovnyak, Nat. Phys. **14**, 213 (2018).

[52] G. Gitgeatpong, Y. Zhao, P. Piyawongwatthana, Y. Qiu, L. W. Harriger, N. P. Butch, T. J. Sato, and K. Matan, Phys. Rev. Lett. **119**, 047201 (2017).

[53] S. Meyer, B. Dupé, P. Ferriani, and S. Heinze, Phys. Rev. B **96**, 094408 (2017).

[54] A. Qaiumzadeh, I. A. Ado, R. A. Duine, M. Titov, and A. Brataas, Phys. Rev. Lett. **120**, 197202 (2018).

[55] M. Bode, M. Heide, K. von Bergmann, P. Ferriani, S. Heinze, G. Bihlmayer, A. Kubetzka, O. Pietzsch, S. Blügel, and R. Wiesendanger, Nature (London) **447**, 190 (2007).

[56] J. Spethmann, S. Meyer, K. von Bergmann, R. Wiesendanger, S. Heinze, and A. Kubetzka, Phys. Rev. Lett. **124**, 227203 (2020).

[57] H. Yan, Z. Feng, S. Shang, X. Wang, Z. Hu, J. Wang, Z. Zhu, H. Wang, Z. Chen, H. Hua, W. Lu, J. Wang, P. Qin, H. Guo, X. Zhou, Z. Leng, Z. Liu, C. Jiang, M. Coey, and Z. Liu, Nat. Nanotechnol. **14**, 131 (2019).

[58] L. Pál, E. Krén, G. Kádár, P. Szabó, and T. Tarnóczi, J. Appl. Phys. **39**, 538 (1968).

[59] Q. Li, J. H. Liang, Y. M. Luo, Z. Ding, T. Gu, Z. Hu, C. Y. Hua, H. J. Lin, T. W. Pi, S. P. Kang, C. Won, and Y. Z. Wu, Sci. Rep. **6**, 22355 (2016).

[60] K. Arai, T. Okuda, A. Tanaka, M. Kotsugi, K. Fukumoto, T. Ohkochi, T. Nakamura, T. Matsushita, T. Muro, M. Oura, Y. Senba, H. Ohashi, A. Kakizaki, C. Mitsumata, and T. Kinoshita, Phys. Rev. B **85**, 104418 (2012).

[61] J. Das and K. S. Menon, J. Magn. Magn. Mater. **449**, 415 (2018).

[62] H. W. Chang, F. T. Yuan, P. Y. Yeh, Y. C. Chen, Y. L. Lai, P. H. Pan, C. R. Wang, L. Horng, and W. C. Chang, AIP Adv. **9**, 035330 (2019).

[63] T. Chatterji, G. J. McIntyre, and P. A. Lindgard, Phys. Rev. B **79**, 172403 (2009).

[64] N. R. Montes, P. Gorria, D. M. Blanco, A. B. Fuertes, I. P. Orench, L. Olivi, and J. A. Blanco, AIP Adv. **6**, 056104 (2016).

[65] G. Kresse and J. Hafner, Phys. Rev. B **47**, 558 (1993).

[66] P. E. Blochl, Phys. Rev. B **50**, 17953 (1994).

[67] J. P. Perdew, K. Burke, and M. Ernzerhof, Phys. Rev. Lett. **77**, 3865 (1996).

[68] H. Yang, A. Thiaville, S. Rohart, A. Fert, and M. Chshiev, Phys. Rev. Lett. **115**, 267210 (2015).

[69] H. Yang, O. Boulle, V. Cros, A. Fert, and M. Chshiev, Sci. Rep. **8**, 12356 (2018).

[70] H. Yang, G. Chen, A. A. C. Cotta, A. T. N'Diaye, S. A. Nikolaev, E. A. Soares, W. A. A. Macedo, K. Liu, A. K. Schmid, A. Fert, and M. Chshiev, Nat. Mater. **17**, 605 (2018).

[71] M. Heide, G. Bihlmayer, and S. Blügel, Phys. Rev. B **78**, 140403(R) (2008).

[72] V. Kashid, T. Schena, B. Zimmermann, Y. Mokrousov, S. Blügel, V. Shah, and H. G. Salunke, Phys. Rev. B **90**, 054412 (2014).

[73] S. Mankovsky, S. Polesya, and H. Ebert, Phys. Rev. B **99**, 104427 (2019).

[74] P. Kurz, F. Förster, L. Nordström, G. Bihlmayer, and S. Blügel, Phys. Rev. B **69**, 024415 (2004).

[75] B. Zimmermann, M. Heide, G. Bihlmayer, and S. Blügel, Phys. Rev. B **90**, 115427 (2014).

[76] B. Zimmermann, G. Bihlmayer, M. Böttcher, M. Bouhassoune, S. Lounis, J. Sinova, S. Heinze, S. Blügel, and B. Dupé, Phys. Rev. B **99**, 214426 (2019).

[77] A. Soumyanarayanan, M. Raju, A. L. Gonzalez Oyarce, A. K. C. Tan, M.-Y. Im, A. P. Petrović, P. Ho, K. H. Khoo, M. Tran, C. K. Gan, F. Ernult, and C. Panagopoulos, Nat. Mater. **16**, 898 (2017).

[78] B. Schweflinghaus, B. Zimmermann, M. Heide, G. Bihlmayer, and S. Blügel, Phys. Rev. B **94**, 024403 (2016).

[79] M. Toyoda, K. Yamauchi, and T. Oguchi, Phys. Rev. B **87**, 224430 (2013).

[80] H. J. Xiang, E. J. Kan, S.-H. Wei, M.-H. Whangbo, and X. G. Gong, Phys. Rev. B **84**, 224429 (2011).

[81] A. Belabbes, G. Bihlmayer, F. Bechstedt, S. Blugel, and A. Manchon, Phys. Rev. Lett. **117**, 247202 (2016).

[82] J. Cho, N. H. Kim, S. Lee, J. S. Kim, R. Lavrijsen, A. Solignac, Y. Yin, D. S. Han, N. J. J. Hoof, H. J. M. Swagten, B. Koopmans, and C. Y. You, Nat. Commun. **6**, 7635 (2015).

[83] E. Simon, K. Palotás, L. Rózsa, L. Udvardi, and L. Szunyogh, Phys. Rev. B **90**, 094410 (2014).

[84] B. Dupé, M. Hoffmann, C. Paillard, and S. Heinze, Nat. Commun. **5**, 4020 (2014).

[85] D. M. Crum, M. Bouhassoune, J. Bouaziz, B. Schweflinghaus, S. Blügel, and S. Lounis, Nat. Commun. **6**, 8541 (2015).

[86] S. Tacchi, R. E. Troncoso, M. Ahlberg, G. Gubbiotti, M. Madami, J. Åkerman, and P. Landeros, Phys. Rev. Lett. **118**, 147201 (2017).

[87] E. Krén, G. Kádár, L. Pál, J. Sólyom, P. Szabó, and T. Tarnóczi, Phys. Rev. **171**, 574 (1968).

[88] C. S. Severin, C. W. Chen, and C. Stassis, J. Appl. Phys. **50**, 4259 (1979).

[89] S. K. Kwon and B. I. Min, Phys. Rev. B **62**, 73 (2000).

[90] K. Ishigami, K. Yoshimatsu, D. Toyota, M. Takizawa, T. Yoshida, G. Shibata, T. Harano, Y. Takahashi, T. Kadono, V. K. Verma, V. R. Singh, Y. Takeda, T. Okane, Y. Saitoh, H. Yamagami, T. Koide, M. Oshima, H. Kumigashira, and A. Fujimori, Phys. Rev. B **92**, 064402 (2015).

[91] T. Ueno, J. Sinha, N. Inami, Y. Takeichi, S. Mitani, K. Ono, and M. Hayashi, Sci. Rep. **5**, 14858 (2015).

[92] S. Kim, K. Ueda, G. Go, P. H. Jang, K. J. Lee, A. Belabbes, A. Manchon, M. Suzuki, Y. Kotani, T. Nakamura, K. Nakamura, T. Koyama, D. Chiba, K. T. Yamada, D. H. Kim, T. Moriyama, K. J. Kim, and T. Ono, Nat. Commun. **9**, 1648 (2018).

[93] X. Ma, G. Yu, C. Tang, X. Li, C. He, J. Shi, K. L. Wang, and X. Li, Phys. Rev. Lett. **120**, 157204 (2018).

[94] J. Towns, T. Cockerill, M. Dahan, I. Foster, K. Gaither, A. Grimshaw, V. Hazlewood, S. Lathrop, D. Lifka, G. D. Peterson *et al.*, Comput. Sci. Eng. **16**, 62 (2014).